CrystEngComm

Accepted Manuscript

ROYAL SOCIETY OF CHEMISTRY

www.rsc.org/crystengcomm

Journal Name RSCPublishing

ARTICLE

A New Route to Fabricate LaOI:Yb^{3+}/Er^{3+} Nanostructures via Inheriting the Morphologies of Precursors

Shang Wu, Wensheng Yu, Xiangting Dong*, Jinxian Wang, Guixia Liu

Cite this: DOI: 10.1039/x0xx00000x

Received 00th January 2012,
Accepted 00th January 2012

DOI: 10.1039/x0xx00000x

www.rsc.org/

LaOI:Yb^{3+}/Er^{3+} nanostructures, including nanofibers and nanobelts, were successfully synthesized by electrospinning combined with a double-crucible iodination method using NH_4I as iodine source. X-ray diffractometry (XRD) analysis reveals that LaOI: Yb^{3+}/Er^{3+} nanostructures are tetragonal in structure with space group of P4/nmm. Scanning electron microscope (SEM) analysis shows that the diameter of LaOI:Yb^{3+}/Er^{3+} nanofibers, the width and thickness of LaOI:Yb^{3+}/Er^{3+} nanobelts are respectively 147.48±17.50 nm, 1.95±0.20 μm and 350 nm under the 95% confidence level. Up-conversion (UC) emission spectrum analysis manifests that LaOI:Yb^{3+}/Er^{3+} nanostructures emit strong green and red up-conversion emissions centering at 523 nm, 540 nm and 667 nm under the excitation of a 980-nm diode laser (DL), which respectively attributed to $^2H_{11/2}\rightarrow{}^4I_{15/2}$, $^4S_{3/2}\rightarrow{}^4I_{15/2}$ and $^4F_{9/2}\rightarrow{}^4I_{I5/2}$ energy levels transitions of Er^{3+} under the excitation of a 980-nm diode laser (DL). It is found that the relative intensities of green and red emission vary obviously with changing the molar concentration of Er^{3+} ions, the optimum molar ratio of Yb^{3+} to Er^{3+} is 10:5 in the as-prepared LaOI:Yb^{3+}/Er^{3+} nanofibers. The possible formation mechanisms of LaOI:Yb^{3+}/Er^{3+} nanofibers and nanobelts are also proposed.

1 Introduction

Lanthanide ions (Ln^{3+}) doped luminescent materials have been extensively studied due to their fascinating optical characteristics, chemical and thermal stabilities.[1-8] In particular, Ln^{3+} doped up-conversion luminescence materials have many potential applications in photonics, LCD back lighting, advanced optical amplifiers and imaging as a result of their low effective density, low phonon energy.[9-13] Among these lanthanide ions, the trivalent erbium ions (Er^{3+}) are the most popular and suitable candidates for the UC processes due to their superior chemical and optical properties, such as large Stokes shifts, multicolor emission and narrow emission spectral lines that can cover the whole visible light region.[14] Ytterbium ion (Yb^{3+}), having a strong and broad absorption band matching well with the emission wavelength of the diode laser, was reported as an excellent sensitizer for the Er^{3+}-activated optical materials.[15] Up to now, many Yb^{3+}/Er^{3+} co-doped materials have been synthesized, including YF_3:Yb/Er nanoparticles,[16] YVO_4:Yb,Er nanoparticles,[17] LaF_3:Yb/Er crystals,[18] YF_3:Yb^{3+}/Er^{3+} hollow nanofibers,[19] etc.

Electrospinning technology has been extensively explored as a simple and versatile method for forming inorganic superfine nanofibers using polymer/inorganic composite as the precursor. The morphology of the electrospun nanomaterials can be controlled by adjusting experimental conditions, such as the spinning solution viscosity, relative air humidity, the structure of spinneret, spinning voltage, and the distance between the spinneret and the collector.[20-22]

Nanofiber and nanobelt are new kinds of one-dimensional nanomaterials with special morphologies. They have attracted increasing interest of scientists owing to their anisotropy, large length-to-diameter ratio and width-to-thickness ratio, unique optical, electrical and magnetic performances.[23-28] Research on the fabrication and properties of nanofibers and nanobelts has become one of the popular subjects of study in the realm of nanomaterials.

Rare earth (RE) oxyhalides with low phonon energies are excellent host materials for lanthanide ions luminescence. REOI has lower phonon energies than REOBr due to the larger atomic mass of I^- than Br^-, so REOI could be used as an effective host for RE activators and may have potential application in manufacturing X-ray intensifying screen.[29-32] So far, LaOI bulk powders have been prepared via direct solid-state reaction at high temperature.[33,34] Youmo Li prepared LaOI bulk powders as follows: La_2O_3 and NH_4I were mixed and reacted under argon flow at 1000 °C for 10 h, or KI and KNO_3 were added into the starting mixture as cosolvent.[33] Yetta D. Eagleman et al. also prepared LaOI powders using the following method: La_2O_3 and LaI_3 powders were mixed in capped alumina tubes, and acted under 3% H_2/argon flow at 1000 °C for 10 h, and thus LaOI were synthesized.[34] Nevertheless, LaOI:Yb^{3+}/Er^{3+} one-dimensional nanomaterials cannot be easily prepared using above process, Once La_2O_3:Yb^{3+}/Er^{3+} one-dimensional nanostructures are directly mixed with NH_4I powders, the one-dimensional nanostructures will be cut into pieces by the melted NH_4I, and the morphology of La_2O_3:Yb^{3+}/Er^{3+} one-dimensional nanostructures cannot be remained. Hence, traditional solid-state method is not suitable for preparing LaOI:Yb^{3+}/Er^{3+} one-dimensional nanostructures and the fabrication of pure-phase LaOI:Yb^{3+}/Er^{3+} one-dimensional nanostructures remains a challenging and meaningful subject of study. In order to solve this problem, a

double-crucible method was used for inheriting the morphologies of the La_2O_3:Yb^{3+}/Er^{3+} nanofibers and nanobelts used as precursors, and it is expected that unbroken LaOI:Yb^{3+}/Er^{3+} nanofibers and nanobelts will be obtained.

In this paper, LaOI:Yb^{3+}/Er^{3+} nanofibers and nanobelts were fabricated by double-crucible iodination of the La_2O_3:Yb^{3+}/Er^{3+} nanofibers and nanobelts which was fabricated by calcining the electrospun polyvinyl pyrrolidone (PVP)/[$La(NO_3)_3$+$Yb(NO_3)_3$+$Er(NO_3)_3$] composites under argon atmosphere. The morphology, structure and up-conversion (UC) photoluminescence properties of the resulting samples were investigated in detail. In addition, the formation mechanism of LaOI:Yb^{3+}/Er^{3+} nanostructures were also presented.

2 Experimental Section

2.1 Chemicals

Lanthanum oxide (La_2O_3, 99.99%), erbium oxide (Er_2O_3, 99.99%) and ytterbium oxide (Yb_2O_3, 99.99%) were supplied by China Pharmaceutical Group Shanghai Chemical Reagent Company. Ammonium iodide (NH_4I, AR) was obtained from China Pharmaceutical Group Chemical Reagent Company. N, N-dimethylformamide (DMF, AR) and polyvinyl pyrrolidone (PVP, M_w=1 300 000) were purchased from Tianjin Tiantai Chemical Co. Ltd. Nitric acid (HNO_3, AR) was purchased from Beijing chemical plant. All chemicals were directly used as received without further purification.

2.2 Preparation of LaOI:Yb^{3+}/Er^{3+} nanofibers

LaOI:10%Yb^{3+}/x%Er^{3+} nanofibers [x= 10, 5, 3 and 1, x stands for molar ratio of Er^{3+}/(Yb^{3+}+Er^{3+}+La^{3+})] were prepared by calcinating the electrospun PVP/[$La(NO_3)_3$+$Yb(NO_3)_3$+$Er(NO_3)_3$] composite nanofibers, followed by iodinating the calcinated products. In the typical procedure of preparing representative LaOI:10%Yb^{3+}/5%Er^{3+} nanofibers, 0.7558 g of La_2O_3, 0.0522 g of Er_2O_3 and 0.1084 g of Yb_2O_3 were dissolved in HNO_3 to form $RE(NO_3)_3{\cdot}6H_2O$ (RE=La, Er and Yb) via evaporating excess HNO_3 and water by heating, then the $RE(NO_3)_3{\cdot}nH_2O$ (RE = La, Er and Yb, n-unknown molecules of the water) powders were dissolved in DMF, and 1.8012 g of PVP was added into the above solution. In this spinning solution, the mass ratios of rare earth nitrates, DMF and PVP were equal to 9:82:9, the dosages of used materials were summarized in **Table 1**. The mixture was magnetically stirred to form a homogeneous spinning solution. The PVP/[$La(NO_3)_3$+$Yb(NO_3)_3$+$Er(NO_3)_3$] composite nanofibers were obtained by electrospinning of the above spinning solution at room temperature under the direct current high-voltage of 12.4 kV, the distance between the spinneret and collector was fixed at 20 cm, and the angle between spinneret and horizon was fixed to 15°. La_2O_3:Yb^{3+}/Er^{3+} nanofibers were prepared by calcining the electrospun composites nanofibers at 700 °C for 8 h with a heating rate of 1 °C/min in air.

LaOI:10%Yb^{3+}/5%Er^{3+} nanofibers were prepared by iodating the obtained La_2O_3:10%Yb^{3+}/5%Er^{3+} nanofibers with NH_4I as iodization agent as following: small amount of NH_4I powders was loaded into a small crucible, and some carbon rods were put on the surface of the NH_4I powders, then La_2O_3:10%Yb^{3+}/5%Er^{3+} nanofibers were loaded on the carbon rods, thus NH_4I powders and La_2O_3:10%Yb^{3+}/5%Er^{3+} nanofibers were separated by carbon rods which prevented the nanofibers from morphology damage, The small crucible was placed into a big crucible, and then excessive NH_4I was added into the space between the two crucibles, and the big crucible was covered with its lid. The sample was annealed at 800 °C for 4 h with a heating rate of 2 °C/min under argon atmosphere, then the temperature was decreased to 200 °C at a rate of 2 °C/min, followed by naturally down to room temperature. Thus, LaOI:10%Yb^{3+}/5%Er^{3+} nanofibers were successfully acquired. Other series of LaOI:10%Yb^{3+}/x% Er^{3+} [x=1, 3 and 10] nanofibers were prepared by the similar procedure except for different doping molar concentration of Yb^{3+} and Er^{3+}.

2.3 Fabrication of LaOI:10%Yb^{3+}/5%Er^{3+} nanobelts

LaOI:10%Yb^{3+}/5%Er^{3+} nanobelts were formed by adjusting the mass ratios of rare earth nitrates, DMF, PVP and the electrospinning parameters in the above procedures. The compositions of spinning solutions and the experimental parameters were summarized in Table 1. Other preparations processes followed the same procedures as those for preparing for LaOI:10%Yb^{3+}/x%Er^{3+} nanofibers, as described in the section 2.2.

Table 1 Compositions of the spinning solutions and electrospinning parameters

sample	Nitrates (g)	PVP (g)	DMF (g)	Stirring Time(h)	Voltage (kV)	Distance (cm)	Room Temperature(°C)	Relative humidity(%)
nanofibers	1.8	1.8012	16.4096	4	12.4	20	20-25	25-40
nanobelts	1.8	3.2404	13.0437	12	8.0	16	20-25	35-50

3 Characterization

X-ray diffraction (XRD) measurements were carried out using a Rigaku D/max-RA X-ray diffractometer with Cu Ka radiation of 0.15406 nm. The morphologies and sizes of the samples were investigated by an XL-30 field emission scanning electron microscope (SEM) made by FEI Company. The purity of the products was examined by an Oxford ISIS-300 energy dispersive spectrometer (EDS). Up-conversion luminescence spectra of samples were recorded on a Hitachi F-7000 fluorescence spectrophotometer using a Xe lamp as the excitation source.

4 Results and Discussion

4.1 Crystal structure

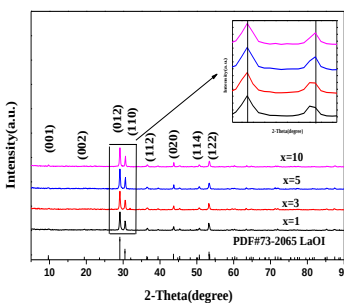

Fig. 1 XRD patterns of LaOI:10%Yb^{3+}/x%Er^{3+} nanofibers (x= 10, 5, 3 and 1) with PDF standard card of LaOI

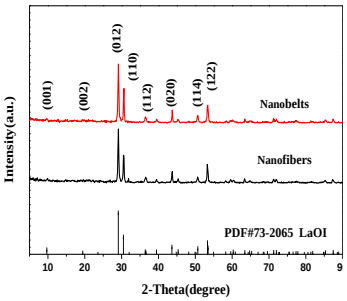

Fig. 2 XRD patterns of LaOI:10%Yb^{3+}/5%Er^{3+} nanofibers and nanobelts with PDF standard card of LaOI

Fig. 1 shows the XRD patterns of the LaOI:10%Yb^{3+} nanofibers doped with different molar concentration of Er^{3+} ions. As seen from Fig.1, well-defined diffraction peaks are acquired, all of which can be readily indexed to those of the pure phase LaOI with tetragonal structure according to the PDF standard card No.73-2065 (LaOI), and the space group is P4/nmm. The characteristic diffraction peaks are located near 2θ=9.875°, 29.125°, 30.625°, 36.500°, 43.750°, 45.250°, 50.625°, and 53.375°. No diffraction peaks of any other phases or impurities are detected, indicating that crystalline LaOI:10%Yb^{3+}/x%Er^{3+} are obtained, and Er^{3+} and Yb^{3+} ions are effectively built into the host lattice via replacing La^{3+} because of the similar radius between La^{3+} and Yb^{3+}/Er^{3+} [radius (La^{3+}) = 1.061Å, radius (Yb^{3+}) = 0.858Å, radius (Er^{3+}) = 0.881Å]. However, the diffraction peaks of LaOI: 10%Yb^{3+}/x%Er^{3+} nanofibers slightly shift, as seen from the inset of Fig.1. The lattice constants were calculated using the following expression:

$$sin^2\theta=(\lambda/2a)^2\times(h^2+k^2)+(\lambda/2c)^2\times l^2 \quad (1)$$

where λ value is 1.5406Å，h, k and l are diffraction indexes, and the results are summarized in **Table 2**. The same structures are obtained for the LaOI:10%Yb^{3+}/5%Er^{3+} nanofibers and nanobelts, as manifested in Fig.2. The lattice constants of LaOI:10%Yb^{3+}/5%Er^{3+} nanofibers and nanobelts were also calculated using the above expression(1), and the results are summarized in **Table 3**.

Table 2 Lattice constants of LaOI:10%Yb^{3+}/x%Er^{3+} (x=1, 3, 5 and 10) nanofibers

x	2-Theta(degree)	h	k	l	Lattice constants(Å)
1	29.125	0	1	2	a=b=2.1464
	30.5	1	1	0	c=4.6857
3	29.125	0	1	2	a=b=2.1464
	30.5	1	1	0	c=4.6857
5	29.125	0	1	2	a=b=2.1385
	30.625	1	1	0	c=4.7076
10	29.125	0	1	2	a=b=2.1385
	30.625	1	1	0	c=4.7076

Table 3 Lattice constants of LaOI:10%Yb^{3+}/5%Er^{3+} nanofibers and nanobelts

Sample	2-Theta(degree)	h	k	l	Lattice constants(Å)
Nanofibers	29.125	0	1	2	a=b=2.1385
	30.625	1	1	0	c=4.7076
Nanobelts	29.125	0	1	2	a=b=2.1385
	30.625	1	1	0	c=4.7076

4.2 Morphology

Fig. 3 a and b show SEM images of PVP/[$La(NO_3)_3$+$Yb(NO_3)_3$+$Er(NO_3)_3$] composite nanofibers and nanobelts, respectively. As seen from the images, the nanostructures have smooth surface and uniform diameter or width. After annealing at 800°C, as-formed LaOI:10%Yb^{3+}/5%Er^{3+} nanofibers and nanobelts have coarse surface which are shown in **Fig. 3 c and d**. Distribution histograms of diameter and width of the nanostructures are shown in **Fig. 4**. Under the 95% confidence level, the diameter of the nanofibers and the width of the nanobelts analyzed by Shapiro-Wilk method are found to be normal distribution. As seen from **Fig. 4**, the diameter of PVP/[$La(NO_3)_3$+$Yb(NO_3)_3$+$Er(NO_3)_3$] nanofibers and LaOI:10%Yb^{3+}/5%Er^{3+} nanofibers and the width of composite nanobelts and LaOI:10%Yb^{3+}/5%Er^{3+} nanobelts are 228.50±48.32, 147.48±17.50 nm, 2.43±0.4 and 1.95±0.2 μm, respectively. It is found from **Fig. 3 b and d** that the thickness of PVP/[$La(NO_3)_3$+$Yb(NO_3)_3$+$Er(NO_3)_3$] composite nanobelts and LaOI:10%Yb^{3+}/5%Er^{3+} nanobelts are ca. 420 nm and ca. 350 nm, respectively. From **Fig. 4**, it is observed that the diameter of LaOI:Yb^{3+}/Er^{3+} nanofibers is smaller than that of composite nanofibers. Similarly, the width of LaOI:10%Yb^{3+}/5%Er^{3+} nanobelts is smaller than that of composite nanobelts.

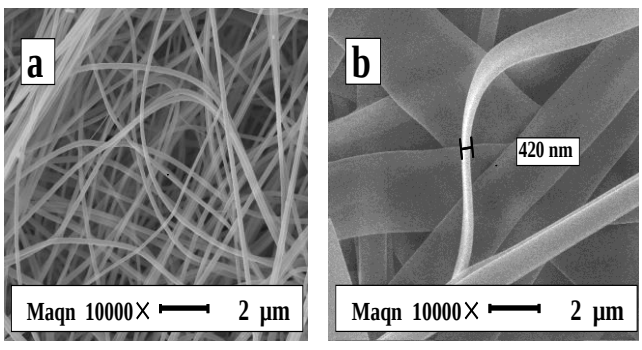

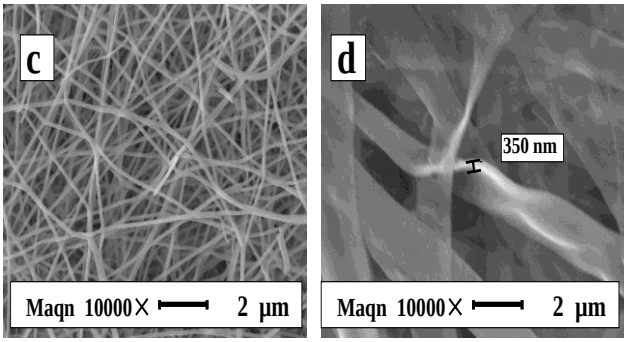

Fig.3 SEM images of PVP/[$La(NO_3)_3$+$Yb(NO_3)_3$+$Er(NO_3)_3$] composite nanofibers (a)，nanobelts (b), LaOI:10%Yb^{3+}/5%Er^{3+} nanofibers (c) and nanobelts (d)

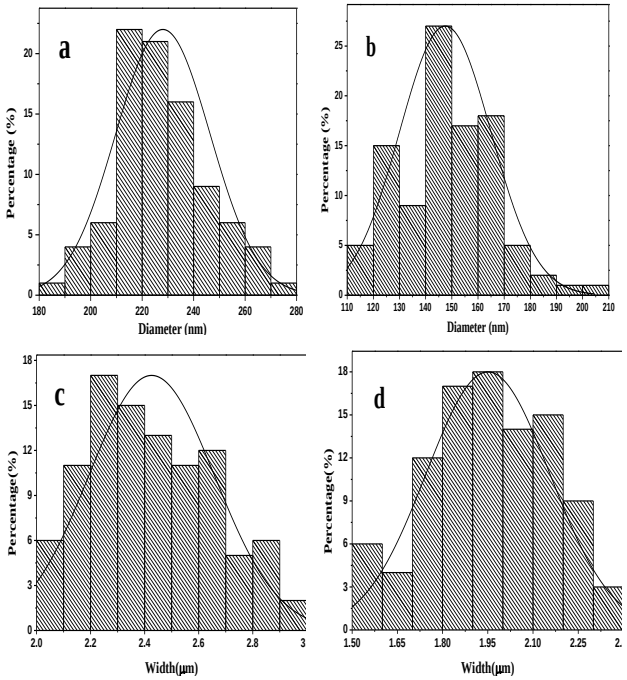

Fig. 4 Distribution histograms of diameter of PVP/[$La(NO_3)_3$+$Yb(NO_3)_3$+$Er(NO_3)_3$] composite fibers (a), LaOI:10%Yb^{3+}/5%Er^{3+} nanofibers (b) and width distribution histograms of composite nanobelts (c) and LaOI:10%Yb^{3+}/5%Er^{3+} nanobelts (d)

4.3 Energy dispersive spectrum analysis

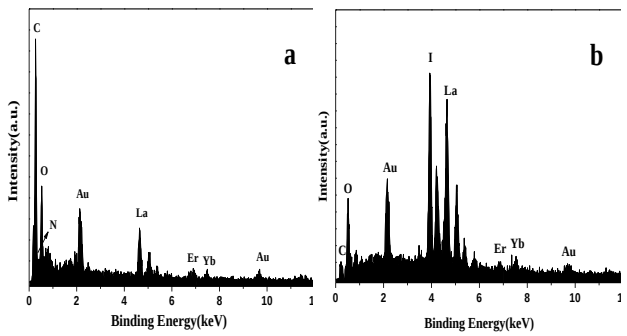

Fig. 5 EDS spectra of PVP/[$La(NO_3)_3$+$Yb(NO_3)_3$+$Er(NO_3)_3$] composite fibers (a) and LaOI:10%Yb^{3+}/5%Er^{3+} nanofibers (b)

EDS spectra of PVP/[$La(NO_3)_3$+$Yb(NO_3)_3$+$Er(NO_3)_3$] and LaOI:10%Yb^{3+}/5%Er^{3+} nanofibers are shown in **Fig. 5**. EDS spectra show that C, N, O, La, Yb and Er are main elements in composite nanofibers, and C, O, I, La, Yb and Er elements exist in LaOI:10%Yb^{3+}/5%Er^{3+} nanofibers. The element C, in the LaOI:10%Yb^{3+}/5%Er^{3+} nanofibers, comes from the used carbon rod. The peak of Au is from the conductive film of Au plated on the sample for SEM observation. The PVP/[$La(NO_3)_3$+$Yb(NO_3)_3$+$Er(NO_3)_3$] composite nanobelts and LaOI:10%Yb^{3+}/5%Er^{3+} nanobelts have the similar EDS spectra compared with the composite nanofibers and LaOI:10%Yb^{3+}/5%Er^{3+} nanofibers. No other elements are found in the samples, indicating that the LaOI:10%Yb^{3+}/5%Er^{3+} nanostructures are highly pure.

4.4 Up-conversion luminescence property

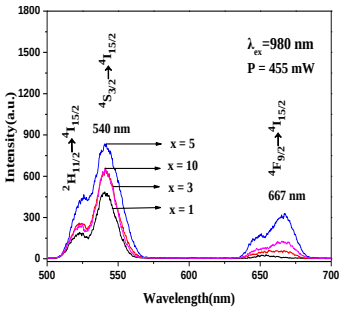

Fig. 6 Up-conversion emission spectra of LaOI: 10%Yb^{3+}/x%Er^{3+} (x= 10, 5, 3 and 1) nanofibers under the excitation of a 980-nm diode laser

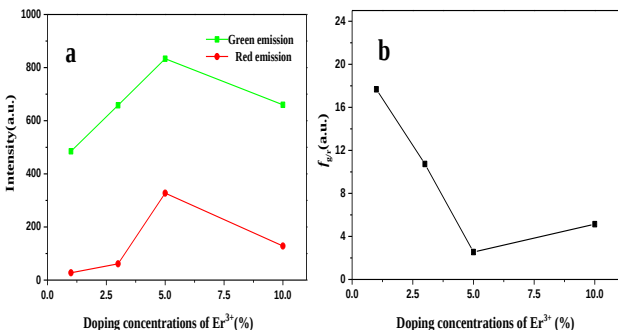

Fig. 7 Variation of the emission intensities (a) and $f_{g/r}$ (the ratio of green to red emission intensity) (b) with doping concentration of Er^{3+} for LaOI:10%Yb^{3+}/x%Er^{3+} (x=10, 5, 3 and 1) nanofibers under the excitation of a 980-nm diode laser

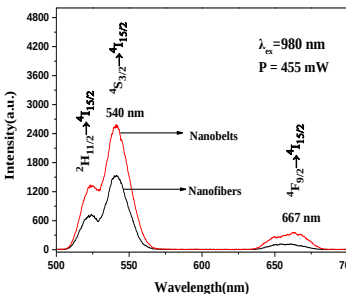

Fig. 8 Up-conversion emission spectra of LaOI:10%Yb^{3+}/5%Er^{3+} nanofibers and nanobelts under the excitation of a 980-nm diode laser

Fig. 6 gives the UC emission spectra of LaOI:10%Yb^{3+}/x%Er^{3+} (x=10, 5, 3 and 1) nanofibers under the excitation of a 980-nm diode laser with the same pump power (in order to avoid the experimental errors). The spectra consist of red emission bands and green emission bands. The red emission bands centering at 667 nm originate from $^4F_{9/2}\rightarrow{}^4I_{15/2}$ energy

levels transition of Er^{3+} ions, and the green emission bands in the region of 520-560 nm are ascribed to the $^2H_{11/2}$, $^4S_{3/2}\rightarrow{}^4I_{15/2}$ energy levels transitions of Er^{3+} ions, respectively. It is found that the relative intensities of green and red emission vary obviously with changing the concentration of Er^{3+} ions. For the LaOI:10%Yb^{3+}/x%Er^{3+} nanofibers, when the concentration of Yb^{3+} is fixed at 10%, the red emission intensity and the green emission intensity increase with Er^{3+} concentration from 1% to 5% and decrease with further increasing in the Er^{3+} concentration from 5% to 10%, as seen in **Fig. 7 a**. The results can be interpreted by the increase of interactions between neighboring Er^{3+} ions with the increase of Er^{3+} ions concentration when Er^{3+} concentration is more than 5%. On the basis of these results, it can be confirmed that the optimized molar ratio of Yb^{3+} to Er^{3+} is 10: 5 in the as-prepared nanofibers. The ratio of green to red emission intensity ($f_{g/r}$) decreases with Er^{3+} concentration from 1% to 5%, and increases with further increasing in the Er^{3+} concentration from 5% to 10%. The $f_{g/r}$ of the LaOI:10%Yb^{3+}/x%Er^{3+} (x=1, 3, 5 and 10) nanofibers are 17.68, 10.73, 2.55 and 5.14, respectively, as shown in **Fig. 7 b**. It seems that the cross-relaxation between Er^{3+} and Yb^{3+} will be increased with the increase of Er^{3+} concentration, causing the population to diminish in $^2H_{11/2}$ (or $^4S_{3/2}$) levels (Er^{3+}) and enhancement of the population in the $^4F_{9/2}$ level (Er^{3+}), leading to the increase of the red emission intensity and decrease of the green emission intensity.[35] **Fig. 8** demonstrates the comparisons among the UC emission spectra of LaOI:10%Yb^{3+}/5%Er^{3+} nanofibers and nanobelts under the excitation of a 980-nm diode laser with the same pump power (455 mW). From **Fig. 8,** one can see that LaOI:10%Yb^{3+}/5%Er^{3+} nanobelts have higher UC emission intensity than that of nanofibers. The result can be interpreted by two diverse factors. Generally, the crystallinity of materials has a crucial impact on the luminescence intensity, the higher the crystallinity, the stronger the UC intensity. The crystallinity of the nanobelts is stronger than that of nanofibers as shown in **Fig.2**. Therefore, the UC emission intensity of the nanobelts is stronger than that of nanofibers. It is known that the specific surface area of materials increases with the decrease of size.[36] A large number of defects are introduced into LaOI:10%Yb^{3+}/5%Er^{3+} nanostructures due to the large surface area. Defects as quenching centers have severe drawback in luminescence intensity for nanomaterials because they provide nonradiative recombination centers for electrons and holes.[37] The specific surface area of the LaOI:10%Yb^{3+}/5%Er^{3+} nanobelts is smaller than that of LaOI:10%Yb^{3+}/5%Er^{3+} nanofibers. Therefore, LaOI:10%Yb^{3+}/5%Er^{3+} nanobelts have the smaller quantity of defects due to the smaller specific surface area, as a result, the nanobelts have the stronger UC intensity.

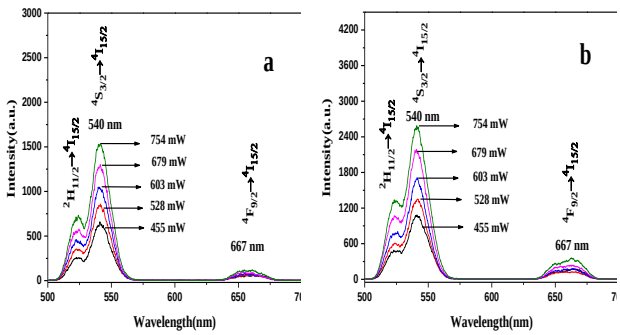

Fig. 9 Up-conversion emission spectra of LaOI: 10%Yb^{3+}/5%Er^{3+} nanofibers (a) and nanobelts (b) under the different pumped power

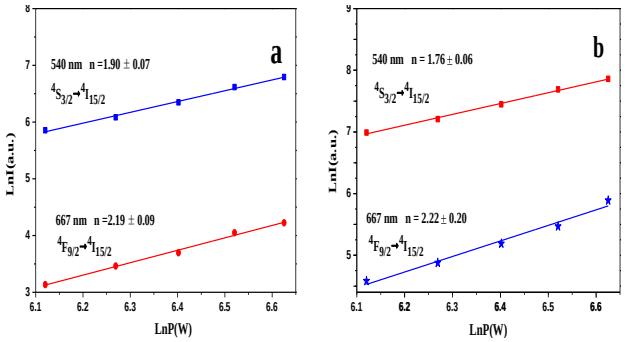

Fig. 10 Plots of natural logarithm intensity of the up-conversion emission (Iup) versus natural logarithm pumped power (P) for LaOI:10%Yb^{3+}/5%Er^{3+} nanofibers (a) and nanobelts (b) a 980-nm diode laser

For the upconversion process, the upconverted emission intensity (I_{up}) depends on the pump power (P) according to the following [38]:

$$_{up} \propto P^n$$

Where n is the number of pump photons required. **Fig. 9** shows the UC emission spectra of the LaOI:10%Yb^{3+}/5%Er^{3+} nanofibers (**a**) and LaOI:10%Yb^{3+}/5%Er^{3+} nanobelts **(b)** under the excitation of a 980-nm DL with different pump power. A plot of natural logarithm I_{up} versus natural logarithm P yields shows a straight line with slope n, as shown in **Fig. 10**. It can be seen that the values of n are 1.90 and 2.19 for the green emission transition ($^4S_{3/2}\rightarrow{}^4I_{15/2}$) and red emission transition ($^4F_{9/2}\rightarrow{}^4I_{15/2}$) of LaOI:10%$Yb^{3+}$/5%$Er^{3+}$ nanofibers, respectively (**in Fig. 10 a**). The slopes (values of n) for the UC luminescence of the green emission transition and the red emission transition for LaOI:10%Yb^{3+}/5%Er^{3+} nanobelts are 1.76 and 2.22, respectively (**in Fig. 10 b)**. Both the slopes for the green and red emissions are about 2, indicating a two-photon emission process is obtained.

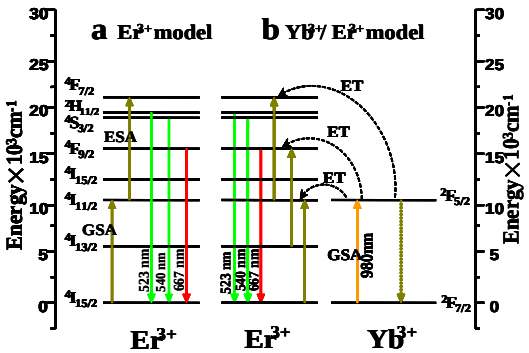

Fig. 11 Simplified energy level scheme of the up-conversion emission mechanism for Yb^{3+}/Er^{3+} co-doped nanostructures

In principle, four basic population mechanisms may be involved in the UC process, namely ground state absorption(GSA), excited state absorption (ESA), energy transfer (ET) and photo avalanche (PA).[35] We can immediately rule out PA as a mechanism of up-conversion in LaOI:Yb^{3+}/Er^{3+} nanostructures because no inflection point is observed in the power study. The two-photon process in LaOI:Yb^{3+}/Er^{3+} nanofibers may happen via the following GSA, ESA and ET processes and their possible schematic diagram is shown in **Fig. 11**. It can be seen that Er^{3+} ions are excited from the ground state ($^4I_{15/2}$) to the $^4I_{11/2}$ state by GSA or ET. When the Yb^{3+} and Er^{3+} ions are co-doped into the host lattices, the ET process become dominant because Yb^{3+} ions have a much larger absorption cross section as compared to that of Er^{3+} around 980 nm.[39] Therefore,

the Er^{3+} ions are excited from the ground state to $^4I_{11/2}$ level by general multi-photon process through the ET from the excited Yb^{3+} ions [$^4I_{15/2}$ (Er)+$^2F_{5/2}$ (Yb)→$^4I_{11/2}$ (Er)+$^2F_{7/2}$ (Yb)]. Then the ions in $^4I_{11/2}$ level rise to $^4F_{7/2}$ level via the ESA or the ET from Yb^{3+} ions to the excited Er^{3+} ions. The electrons in $^4F_{7/2}$ level undergo multi-photon relaxation to the luminescent level $^2H_{11/2}$ and $^4S_{3/2}$ resulting from the small energy gap between them. The radiative transition from $^2H_{11/2}$ and $^4S_{3/2}$ to ground state can result in the green emissions at 523 and 540 nm, respectively. For the red emissions at 667 nm, the electrons at the excited state $^4I_{11/2}$ relax nonradiatively to the $^4I_{13/2}$ level, and then the electrons at $^4I_{13/2}$ level can be excited to the $^4F_{9/2}$ level by the ESA or ET processes from Yb^{3+}. The red emission at 667 nm originates from the transition from the $^4F_{9/2}$ to $^4I_{15/2}$.

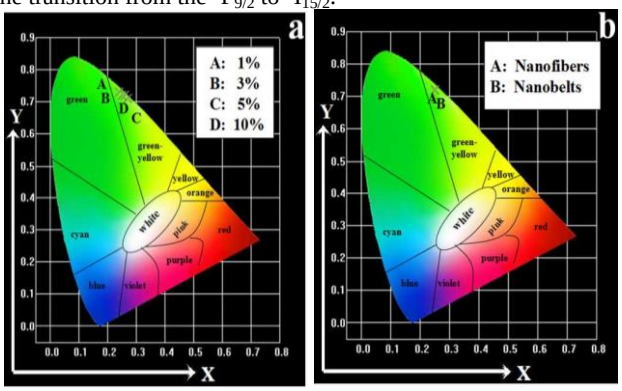

Fig. 12 CIE chromaticity coordinates diagrams for LaOI:10%Yb^{3+}/x%Er^{3+} nanofibers (x = 1, 3, 5 and 10) (a) and LaOI:10%Yb^{3+}/5%Er^{3+} nanofibers and belts (b)

In general, color can be represented by the Commission Internationale de L'Eclairage (CIE) 1931 chromaticity coordinates. **Fig. 12a** shows the chromaticity coordinates of LaOI:10%Yb^{3+}/1%Er^{3+} (0.24, 0.73), LaOI: 10%Yb^{3+}/3%Er^{3+} (0.25, 0.72), LaOI: 10%Yb^{3+}/5%Er^{3+} (0.27, 0.71) and LaOI: 10%Yb^{3+}/10%Er^{3+} (0.26, 0.72) nanofibers. The chromaticity coordinates of LaOI: 10%Yb^{3+}/5%Er^{3+} nanofibers (0.25, 0.72) and nanobelts (0.25, 0.72) are represented in **Fig. 12b**. All of the nanostructures exhibit green-yellow emissions. These results indicate that the color emissions can be tuned by changing the ratio of Yb^{3+} ions and Er^{3+} ions and morphologies of nanostructures. These as-obtained nanostructures could show merits of green-yellow emissions, which is considered to be promising candidates for application in LEDs.

4.5 Formation mechanism for LaOI:Yb^{3+}/Er^{3+} nanostructures

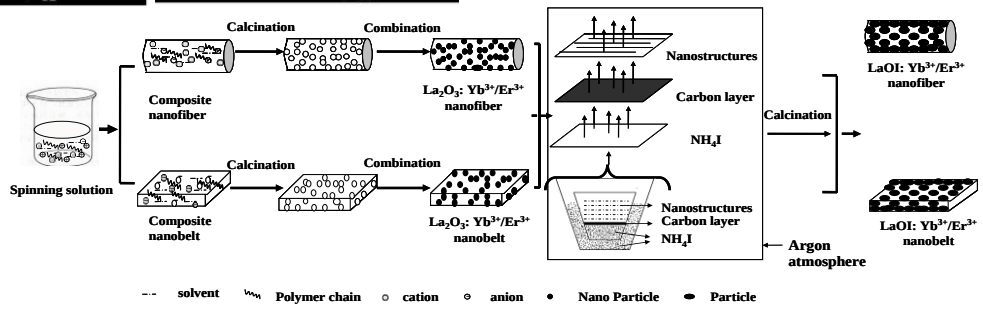

Fig .13 Schematic diagram of formation mechanism of LaOI: Yb^{3+}/Er^{3+} nanofibers and nanobelts

Formation mechanisms of LaOI:Yb^{3+}/Er^{3+} nanostructures are shown in **Fig. 13**. $La(NO_3)_3$, $Yb(NO_3)_3$, $Er(NO_3)_3$ and PVP were mixed with DMF to form spinning solution with certain viscosity. PVP acted as template during the formation of PVP/[$La(NO_3)_3$+$Yb(NO_3)_3$+$Er(NO_3)_3$] composite nanofibers and nanobelts. La^{3+}, Yb^{3+}, Er^{3+} and NO_3^- were mixed or absorbed onto PVP to form composite nanofibers and nanobelts via electrospinning. Some solvent was volatilized in the electrospinning process. PVP, NO_3^- and residual solvent were decomposed and eventually evaporated from the composite fibers and belts during the calcination process. With the increase in the calcining temperature, La^{3+}, Yb^{3+}, Er^{3+} could combine with O_2, coming from air, to form La_2O_3:Yb^{3+}/Er^{3+} crystallites, and then many crystallites were combined into nanoparticles, and finally these nanoparticles were mutually connected to generate La_2O_3:Yb^{3+}/Er^{3+} nanostructures.

La_2O_3:Yb^{3+}/Er^{3+} nanostructures were iodinated using NH_4I as iodination agent. In the iodinated process, NH_4I was decomposed into NH_3 and HI at about 450°C. With the increase of calcination temperature, HI gases reacted with La_2O_3:Yb^{3+}/Er^{3+} nanostructures to produce LaOI:Yb^{3+}/Er^{3+} nanostructures. During the process, NH_4I powders and La_2O_3:Yb^{3+}/Er^{3+} nanostructures were separated by carbon rods which prevented La_2O_3:Yb^{3+}/Er^{3+} nanostructures from morphology damage. Same results are found in the preparation of LaOCl:Nd^{3+} nanostructures (included nanofibers, nanobelts and hollow nanofibers).[40] If La_2O_3:Yb^{3+}/Er^{3+} nanostructures were directly mixed with NH_4I powders, the nanostructures would be cut into pieces by the melted NH_4I, as present in Fig. 14. The double-crucible method we proposed here is actually a solid-gas reaction, which has been proved to be an important method, not only can retain the morphology of La_2O_3:Yb^{3+}/Er^{3+} nanostructures, but also can fabricate LaOI:Yb^{3+}/Er^{3+} nanostructures with pure phase at relatively low temperature. Reaction schemes for formation of LaOI:Yb^{3+}/Er^{3+} nanostructures proceed as follows:

$$PVP/[La(NO_3)_3+Yb(NO_3)_3+Er(NO_3)_3] + O_2 \xrightarrow{700°C} CO_2+H_2O+NO_2+La_2O_3:Yb^{3+}/Er^{3+}$$

$$NH_4I \xrightarrow{450°C} NH_3+HI$$

$$La_2O_3:Yb^{3+}/Er^{3+} + 2\,HI \xrightarrow{800°C} 2\,LaOI:Yb^{3+}/Er^{3+} + H_2O$$

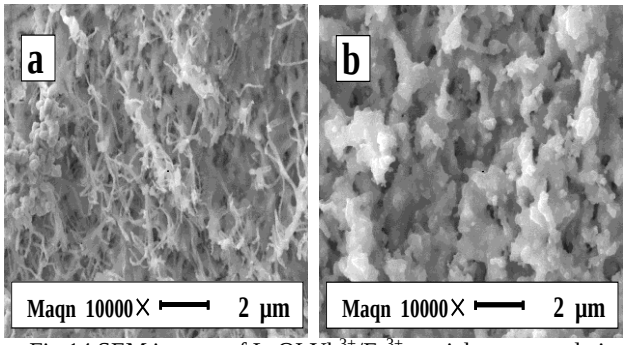

Fig.14 SEM images of LaOI:Yb^{3+}/Er^{3+} particles prepared via direct mixing of La_2O_3:Yb^{3+}/Er^{3+} nanofibers (a) and nanobelts (b) with NH_4I powders

5 Conclusions

Yb^{3+}, Er^{3+} co-doped LaOI nanofibers and nanobelts were synthesized by electrospinning method combined with a double-crucible iodinating method using NH_4I as iodination agent. The diameter of LaOI:Yb^{3+}/Er^{3+} nanofibers is 147.48 ± 17.50 nm, and the width and thickness of LaOI:Yb^{3+}/Er^{3+} nanobelts respectively are 1.95 ± 0.20 μm and 350 nm. Upon the excitation of a 980-nm diode laser, LaOI:Yb^{3+}/Er^{3+} nanostructures emit green and red up-conversion emissions centering at 540 nm and 667 nm, attributed to $^4S_{3/2}\rightarrow{}^4I_{15/2}$ and $^4F_{9/2}\rightarrow{}^4I_{15/2}$ transitions of Er^{3+}, respectively. The up-conversion luminescent mechanism and the formation mechanisms of LaOI:Yb^{3+}/Er^{3+} nanostructures are also proposed.

Acknowledgments

This work was financially supported by the National Natural Science Foundation of China (NSFC 50972020, 51072026), Specialized Research Fund for the Doctoral Program of Higher Education (20102216110002, 20112216120003), the Science and Technology Development Planning Project of Jilin Province (Grant Nos. 20130101001JC, 20070402), the Science and Technology Research Project of the Education Department of Jilin Province during the eleventh five-year plan period(Under grant No. 2010JYT01), Key Research Project of Science and Technology of Ministry of Education of China (Grant No. 207026).

Notes and references

Key Laboratory of Applied Chemistry and Nanotechnology at Universities of Jilin Province, Changchun University of Science and Technology, Changchun 130022. Fax: 86 0431 85383815; Tel: 86 0431 85582574; E-mail: dongxiangting888@163.com

1 X. H. Yin, Q. Zhao, B. Q. Shao, W. Lv, Y. H. Li and H. P. You. *CrystEngComm*, 2014, **DOI:** 10.1039/C3CE42571A.
2 S. Wang, S. Y. Song, R. P. Deng, H. L. Guo, Y. Q. Lei, F. Cao, X. Y. Li, S. Q. Su and H. J. Zhang, *CrystEngComm*, 2010, **12**, 3537-3541.
3 M. Yang, H. P. You, N. Guo, Y. J. Huang, Y. H. Zheng and H. J. Zhang, *CrystEngComm*, 2010, **12**, 4141-4145.
4 G. Jia, H. P. You, Y. H. Zheng, K. Liu, N. Guo and H. J. Zhang, *CrystEngComm*, 2010, **12(10)**, 2943-2948.
5 M. Y. Ding, C. H. Lu, L. H. Cao, Y. R. Ni and Z. Z. Xu, *Analyst*, 2013, **15**, 8366-8373.
6 B. Ding, P. Yang, Y. Y. Liu, Y. Wang and G. X. Du, *Analyst*, 2013, **15**, 2490-2503.
7 G. Jia, G. M. Zhang, S. W. Ding, L. Y. Wang, L. F. Li and H. P. You, *CrystEngComm*, 2012, **14**, 573-578.
8 Q. Zhao, Y. H. Zheng, N. Guo, Y. C. Jia, H. Qiao, W. Z. Lv and H. P. You, *CrystEngComm*, 2012, **14**, 6659-6664.
9 Y. S. Liu, D. T. Tu, H. M. Zhu, R. F. Li, W. Q. Luo and X. Y. Chen, *Adv. Mater.* 2012, **22**, 3266-71.
10 L. Y. Wang and Y. D. Li, *Chem. Mater.* 2007, **19**, 727-734.
11 L. D. Carlos., R. A. S. Ferreira, V. Z. Bermudez and S. J. L Ribeiro, *Adv. Mater.* 2011, **21**, 509-534.
12 L. Y. Yang, J. X. Wang, X. T. Dong, G. X. Liu and W. S. Yu, *J. Mater. Sci.*, 2013, **48**, 644-650.
13 S. Wang, S. Q. Su, S. Y. Song, R. P. Deng and H. J. Zhang, *CrystEngComm*, 2012, **14**, 4266-4269.
14 F. Vetrone, J. C. Boyer and J. A. Capobianco, *J. Phys. Chem. B*, 2001, **106**, 5622-28.
15 F. Y. Weng, D. Q. Chen, Y. S. Wang, Y. L. Yu, P. Huang and H. Lin, *Ceramics Inter.*, 2009, **35**, 2619-2623.
16 R. X. Yan and Y. D. Li , *Adv. Funct. Mater.*, 2005, 15, 763-770.
17 G. Mialon, S. Türkcan, G. Dantelle, D. P. Collins, M. Hadjipanayi, R. A. Taylor, T. Gacoin, A. Alexandrou and J. P. Boilot, *J. Phys. Chem.C*, 2010, **114(51)**, 22449-22454.
18 Y. Wu, D. M. Yang, X. J. Kang, Y. Zhang, S. S. Huang, C. Li and J. Lin, *CrystEngComm*, 2014, 16, 1056-1063.
19 D. Li, X. T. Dong, W. S. Yu, J. X. Wang and G. X. Liu, *J. Nanopart. Res.*, 2013, **15(6)**, 1704-1713.
20 Q. L. Ma, J. X. Wang, X. T. Dong, W. S. Yu, G. X. Liu and J. Xu, *J. Mater. Chem.*, 2012, **22(29)**, 14438-14442.
21 W. W. Ma, X. T. Dong, J. X. Wang, W. S. Yu and G. X. Liu, *J. Mater. Sci.*, 2013, **48(6)**, 2557-2565.
22 D. Q. Shao, J. X. Wang, X. T. Dong, W. S. Yu and G. X. Liu, *J. Mater. Sci.: Mater. El.*, 2013, **24(12)**, 4718-4724.
23 H. F. Xiang, Y. H. Long, X. L. Yu, X. L. Zhang, N. Zhao and J. Xu, *CrystEngComm*, 2011, **13(15)**, 4856-4860.
24 J. H. Zhu, J. M. Song, S. H. Yu, W. Q. Zhang and J. X. Shi, *CrystEngComm*, 2009, **11**, 539-541.
25 M. E. Fragalà, I. Cacciotti, Y. Aleeva, R. Lo Nigro, A. Bianco, G. Malandrino, C. Spinella, G. Pezzotti and G. Gusmano, *CrystEngComm*, 2010, **12**, 3858-3865
26 W. J. Zhou, X. Y. Liu, J. J. Cui, D. Liu, J. Li, H. D. Jiang, J. Y. Wang and H. Liu, *CrystEngComm*, 2011, **13**, 4557-4563
27 M. Zhuo, Y. J. Chen, T. Fu, H. N. Zhang, Z. Xu, Q. H. Li and T. H. Wang, *Nanoscalek*, 2014, **6**, 6521-6525
28 J. W. Zhu and D. F. Xue, *CrystEngComm*, 2014, **16**, 642-648
29 M. S. Islam. *J. Phys. Chem. Solids.*, 1990, **51**, 367-372.
30 J. Hölsä, M. Lastusaari, J. Niittykoski and R. S. Puche, *Phys. Chem. Chem. Phys*., 2002, **4**, 3091-3097.
31 D. Y. Wang, Y. Y. Guo, E. D. Zhang, X. B. Chao, L. S. Yu, J. L. Luo, W. P. Zhang and M. Yin, *J. Alloys Compd.*, 2005, **397**, 1–4.
32 D. Y. Wang, W. P. Zhang and M. Yin, *Opt. Mater*., 2004, **27**, 605-608
33 Y. D. Eagleman, E. B. Courchesne and S. E. Derenzo, *J. Lumin.*, 2011, **131**, 669–675.
34 Y. M. Li, H. D. Lu, J. W. Li and X. G. Miao, *J. Lumin.*, 1986, **35**, 107–109.
35 W. W. Ma, W. S. Yu , X. T. Dong, J. X. Wang and G. X. Liu, *Lumin.*, 2014, **DOI**: 10.1002/bio.2640.
36 K. Kömpe, O. Lehmann and M. Haase, *Chem. Mater*., 2006, **18(18)**, 4442-4446.
37 J. Yang, C. X. Li, Z. W. Quan, C. M. Zhang, P. P. Yang, Y. Y. Li, C. C. Yu and J. Lin, *J. Phys. Chem. C*, 2008, **112(33)**, 12777-12785.
38 Z. Chouahda, J. P. Jouart, T. Duvaut and M. Diaf, *J. Physics: Condens. Mat*., 2009, **21(24)**, 245504.
39 Y. H. Song, Y. J. Huang, L. H. Zhang, Y. H. Zheng, N. Guo and H. P. You, *RSC Adv*. 2012, **2**, 4777-4781.
40 Q. L. Kong, J. X. Wang, X. T. Dong, W. S. Yu and G. X. Liu, *Mater. Express*, 2014, **4**, 13-22.

Revised Graphical Abstract

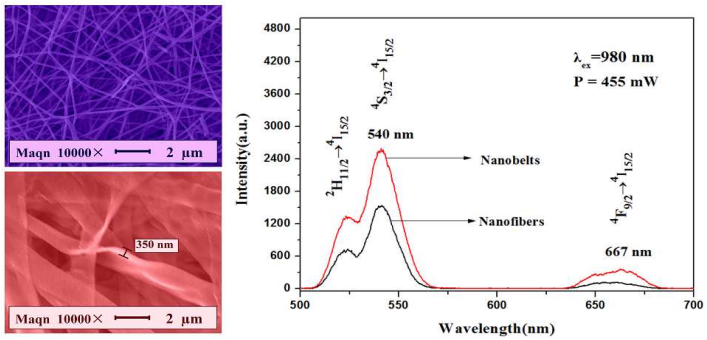

LaOI:Yb^{3+}/Er^{3+} nanofibers and nanobelts have been successfully synthesized via inheriting the morphologies of precursors and exhibit excellent up-conversion luminescence properties.